## 5.4 CT Number Accuracy and Noise

In many clinical practices, radiologists rely on the value of measured CT numbers to differentiate healthy tissue from disease pathology. Although this practice is not recommended by most CT manufacturers (unless the difference between the healthy and diseased tissues is large), it underlines the importance of producing accurate CT numbers. Two aspects factor into CT number accuracy: CT number consistency and uniformity. CT number consistency dictates that if the same phantom is scanned with different slice thicknesses, at different times, or in the presence of other objects, the CT numbers of the reconstructed phantom should not be affected. CT number uniformity dictates that for a uniform phantom, the CT number measurement should not change with the location of the selected ROI or with the phantom position relative to the iso-center of the scanner. For illustration, Fig. 5.30 shows a reconstructed 20-cm water phantom. The average CT numbers in two ROI locations should be identical. Because of the effects of beam hardening, scatter, CT system stability, and many other factors, both CT number consistency and uniformity can be maintained within only a reasonable range. As long as radiologists understand the system limitations and the factors that influence the performance, the pitfalls of using absolute CT numbers for diagnosis can be avoided.

It is important to point out that the CT number may change significantly with different reconstruction algorithms. Most kernels used for reconstruction

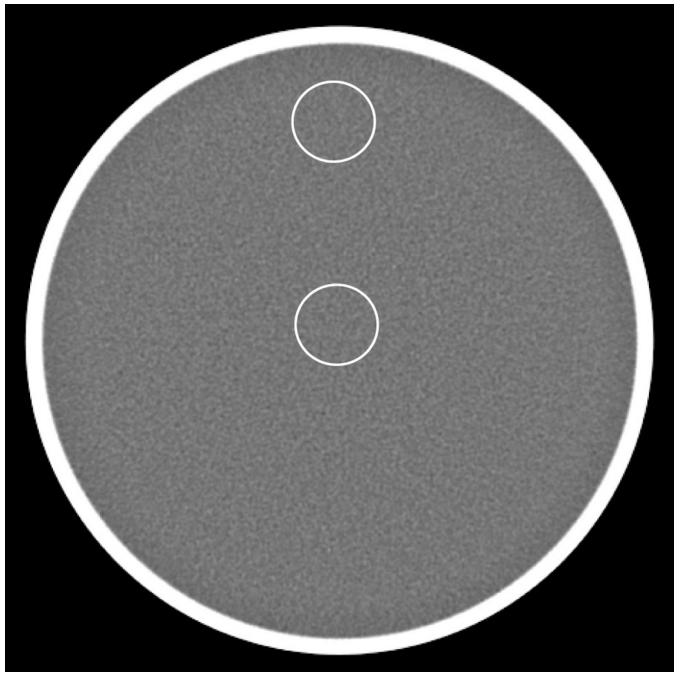

**Figure 5.30** Water phantom for CT number uniformity and noise measurement.

are designed for specific clinical applications and should not be used indiscriminately for all applications. For example, the bone or lung algorithm on HiSpeed™ or LightSpeed™ scanners is designed to enhance the visibility of fine structures of bony objects. It was designed with inherent edge enhancement characteristics and not intended to maintain the CT number accuracy of small objects. Consequently, some of the lung nodules reconstructed with the bone or lung algorithm appear to be falsely calcified, since the CT number of the nodules is artificially elevated. Figures 5.31(a)–(c) depict a chest scan reconstructed with, respectively, the standard algorithm, the lung algorithm, and the difference image. The CT number of many lung nodules and even some large vessels is significantly higher for the lung algorithm, as indicated by the bright structures in the difference image.

With the recent advancements in CT technology (to be discussed in a later chapter), the CT number uniformity requirement needs to be extended from 2D axial images ($x$-$y$ plane) to volumetric 3D images ($x$-$y$-$z$), since state-of-the-art CT scanners cover a large object volume in a single rotation. Similar to the CT number uniformity and accuracy test for the $x$-$y$ plane where a uniform phantom, such as 20-cm water, is used, CT number along the $z$ dimension can be tested with phantoms that are constant in $z$. As an illustration, Fig. 5.32(a) depicts a cylindrical phantom with uniform iodine-rod inserts. To test the CT number uniformity, coronal images are generated, and the average CT numbers are measured at different ROI locations along the phantom. Because the phantom is constant in $z$, the CT number difference reflects the scanner's performance in maintaining CT number accuracy. Figure 5.32(b) depicts coronal/sagittal images formed across the diameters of

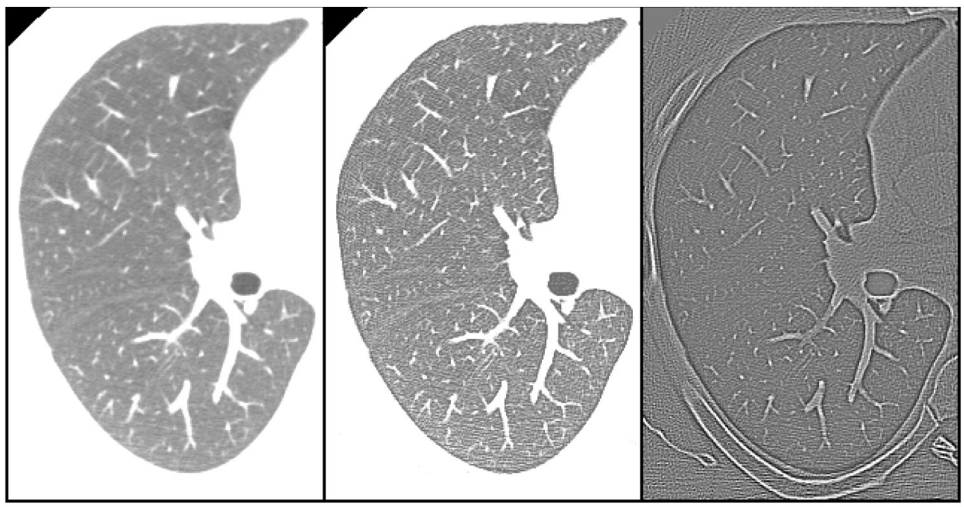


**Figure 5.31** Patient chest scan reconstructed with different algorithms (WW = 1000): (a) standard algorithm, (b) lung algorithm, and (c) difference image.

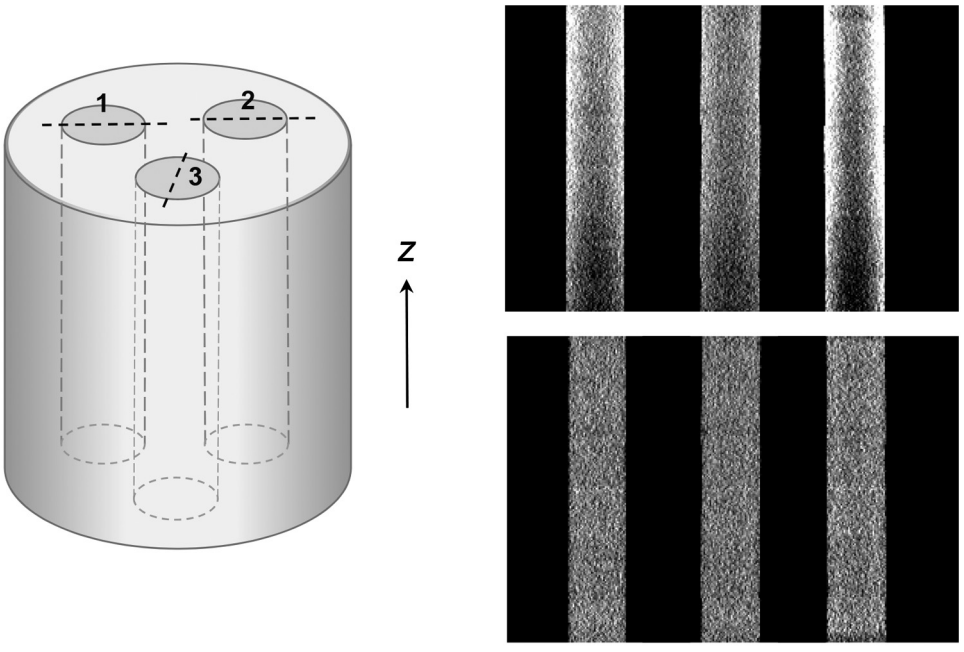


**Figure 5.32** (a) Cylindrical phantom with different concentrations of iodine inserts. (b) Coronal images acquired on a wide-cone CT scanner with different calibrations. (Top): Coronal image of the phantom at the location shown by the dashed lines acquired on a wide-cone CT scanner without proper calibration. The CT number difference between the top and bottom ROIs is about 20 HU. (Bottom): Coronal image of the phantom at the location shown by the dashed lines acquired on a wide-cone CT scanner with proper calibration. The CT number difference between the top and bottom ROIs is about 2 HU.

the rods, with the top portion representing reformatted images without the proper calibration, and the bottom portion representing reformatted images with the proper calibration. It is clear that the bottom image performs better than the top image in terms of CT number uniformity.

Another important performance parameter is image noise, which is typically measured on uniform phantoms. To perform noise measurement, the standard deviation $\sigma$ within an ROI of a reconstructed image $f_{i,j}$ is calculated by

$$\sigma = \sqrt{\frac{\sum_{i,\, j \in \mathrm{ROI}} (f_{i,j} - \bar{f})^2}{N - 1}}, \tag{5.7}$$

where $i$ and $j$ are indexes of the 2D image, $N$ is the total number of pixels inside the ROI, and $f$ is the average pixel intensity that is calculated by

$$\bar{f} = \frac{1}{N} \sum_{i,j \in \mathrm{ROI}} f_{i,\, j}. \tag{5.8}$$

Note that in both equations, the summation is 2D over the ROI. For reliability, several ROIs are often used, and the average value of the measured standard deviations is reported. Ideally, noise measurements should be performed over an ensemble of reconstructed CT images of the same phantom under identical scan conditions to remove the impact of the correlated nature of the CT image noise and the potential biases due to image artifacts resulting from nonperfect system calibration. In such calculations, the summation over ROI shown in Eqs. (5.7) and (5.8) is replaced by the summation over the corresponding ROI of the difference image. Since the difference image is generated by subtracting two images acquired and reconstructed under identical conditions, image artifacts are subtracted out. The resulting standard deviation, of course, needs to be scaled down to reflect the noise level in the original image.

In general, three major sources contribute to the noise in an image. The first source is quantum noise, determined by the x-ray flux or the number of x-ray photons that are detected. This source is influenced by two main factors: the scanning technique (x-ray tube voltage, tube current, slice thickness, scan speed, helical pitch, etc.), and the scanner efficiency [detector quantum detection efficiency (QDE), detector geometric detection efficiency (GDE), umbra-penumbra ratio, etc.]. The scanning technique determines the number of x-ray photons that reach the patient, and the scanner efficiency determines the percentage of the x-ray photons exiting the patient that convert to useful signals. For CT operators, the choices are limited to the scanning protocols. To reduce noise in an image, one can increase the x-ray tube current, x-ray tube voltage, or slice thickness, or reduce the scan speed or helical pitch. The operator must understand the tradeoffs for each choice. For example, although an increased tube voltage helps to reduce noise under an equivalent kW (the product of the tube current and the tube voltage) condition, LCD is generally reduced. Similarly, increased slice thickness may result in a degraded 3D image quality and increased partial-volume effect. A slower scan speed could lead to increased patient motion artifacts and reduced organ coverage. An increased tube current leads to increased patient dose and increased tube loading. As long as the tradeoffs are well understood, these options can be used effectively to combat noise.

The second source that contributes to the noise in an image is the inherent physical limitations of the system. These include the electronic noise in the detector photodiode, electronic noise in the data acquisition system, x-ray translucency of the scanned object, scattered radiation, and many other factors. For CT operators, options to reduce noise in this category are limited.

The third noise-contributing factor is the image generation process. This process can be further divided into different areas: reconstruction algorithms, reconstruction parameters, and effectiveness of calibration. The impact of different classes of reconstruction algorithms on noise was discussed in

Chapter 3 (e.g., see Fig. 3.50) and will not be repeated here. For the same reconstruction algorithm, such as FBP, the reconstruction parameters include the selection of different reconstruction filter kernels, reconstruction FOV, image matrix size, and postprocessing techniques. In general, a high-resolution reconstruction kernel produces an increased noise level. This is mainly because these kernels preserve or enhance high-frequency contents in the projection. Unfortunately, most noise presents itself as high-frequency signals. An example of the filter kernel selection on noise is shown in Fig. 5.15.

A few words should be said about postprocessing techniques. Many image-filtering techniques have been developed over the past few decades for noise suppression. To be effective, these techniques need to not only reduce noise and preserve fine structures in the original image, but also to maintain "natural-looking" noise texture. Often, techniques are rejected by radiologists because the filtered images are too "artificial." In recent years, many advances have been made in this area; a more detailed discussion can be found in Chapter 11 (e.g., Fig. 11.26).

As was discussed in Chapter 3, the calibration or preprocessing techniques used in CT to condition the collected data are not perfect. The residual error often manifests itself as artifacts of small magnitude. These artifacts sometimes cannot be visually detected. However, they do influence the standard deviation measurement and consequently should be considered as part of the noise source.

Although standard deviation is the most straightforward way of measuring noise in an image and correlates fairly well with visual observation, it also has many limitations. As an illustration, Fig. 5.33 shows three images with different types of noise. Figure 5.33(a) shows the noise image of a reconstructed water phantom with the standard kernel. In a similar fashion, the noise image with the bone kernel was scaled, as shown in Fig. 5.33(b). The scaling factor was selected so that Figs. 5.33(a) and (b) have an identical

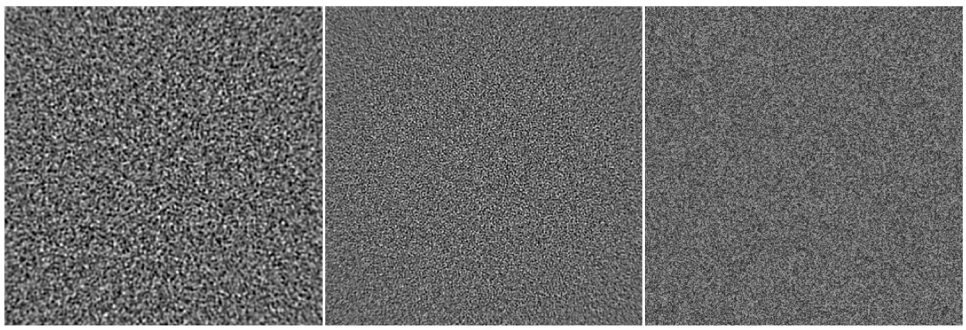


**Figure 5.33** Different types of noises with identical standard deviation ($\sigma = 6.8$). (a) Noise in the reconstructed water phantom with the standard algorithm. (b) Noise in the reconstructed water phantom with the bone algorithm. (c) Additive noise with normal distribution.